PCCP

Accepted Manuscript

ROYAL SOCIETY OF CHEMISTRY

www.rsc.org/pccp

Journal Name

ARTICLE

Photophysical Properties of Octupolar Triazatruxene-Based Chromophores

Received 00th January 20xx,
Accepted 00th January 20xx

DOI: 10.1039/x0xx00000x

www.rsc.org/

Guiying He,[a] Jinjun Shao,[b] Yang Li,[a] Jiangpu Hu,[a] Huaning Zhu,[a] Xian Wang,[a] Qianjin Guo,[a] Chunyan Chi[b,*] and Andong Xia[a,*]

The photophysical properties of three octupolar chromophores containing planar triazatruxene (TAT) as the central electron donor with different electron-withdrawing groups in the tribranched arrangement have been systematically investigated by means of steady state and transient spectroscopy. The multidimensioned intramolecular charge transfer (ICT) properties of these tribranched chromophores related to the observed two-photon absorption (TPA) properties are explored by estimating the TPA essential factors (M_{ge} and $\Delta\mu_{ge}$). Besides the large Stokes shift between steady state absorption and fluorescence spectra in different polar solvents, photoinduced ICT was further demonstrated by quantum-chemical calculations and transient absorption measurements. Both quantum calculations and spectral experiments show that a multidimensional ICT occurs from electron-rich core to the electron-deficient periphery of these TAT derivatives. The results of solvation effects and the dynamics of the excited states show that the excited states of these three chromophores tend to exhibit an excitation localization on one of the dipolar branches, which is beneficial to achieve large M_{ge} and $\Delta\mu_{ge}$, thus leading to enhanced TPA properties.

Introduction

In recent decades, electronic push-pull chromophores with tunable spectral properties have been extensively studied because of their potential applications in a large number of areas, such as organic light-emitting diode (OLED),[1] organic solar cells,[2-4] and two-photon excitation fluorescence imaging.[5-7] The typical organic push-pull chromophores consisting of electron donors and acceptors connected by a π-conjugated bridge (D-B-A) have been extensively developed because their absorption spectra and energy gaps can be easily tuned by controlling the ICT from electron donors to electron acceptors. In comparison with the conventional dipolar molecules, octupolar molecules connecting three ICT moieties through a conjugation bridge have several advantages, while the multidimensional intramolecular charge transfer (MDICT) between core and peripheries in octupolar systems gives rise to many special electronic properties.[8] For example, considering the first hyperpolarizabilities, octupolar molecules is shown 3-8 times larger than that of the corresponding dipolar branches.[9,10] The interaction between branches can lead to enhancement of two-photon absorption with high fluorescence quantum yield.[11-16] A great number of works have done on building π-conjugated octupolar molecules with π-centers and functional groups of electron-donating or electron-withdrawing groups at the terminal sites.[17-19] With different kinds of D-B-A structures, the TPA cross sections can be achieved from hundreds up to larger than 10000 GM.[7,15,20-23] Compared to those octupolar molecules with three-dimensionally twisted cores, octupolar molecules with a planar, extended π-conjugated core are expected to afford better performance because of the rigid and planar conjugation core.[24-27] For example, triazatruxene (TAT) could be a good candidate as a conjugative core with a planar, extended π-conjugated geometry.[17,26] TAT resembles truxene, as a trimer, in which three carbazole units are sharing a benzene ring, leading to an extended π-conjugated coplanar geometry with strong electron-donating ability, where the acceptor groups could be extended along trimeric branches at the terminal sites to further improve photophysical properties. Such types of structures have shown increasing interest in the design and application of the TAT derivatives for two-photon excitation fluorescence,[24,26,28] bulk heterojunction solar cells and OLED.[29-31] In our previous work, we have successfully synthesized several types of TAT-based octupolar molecules, all chromophores (**1-6**) showed high two-photon absorption (TPA) cross sections ranging from 280GM to 1620 GM, in which **TAT-T-Bz** and **TAT-T-PhCN** (see Scheme 1) exhibit the best performance for two-photon excitations.[17]

Based on the Frankel exciton model, octupolar systems such as the TAT series of chromophores with C_3 symmetry could be regarded as three arms with a dipolar donor-acceptor pair in each arm. Within the sum-over-states approach,[14,32,33] the TPA cross-section (δ_{TPA}) into lowest-energy absorption can be expressed as

$$\delta_{TPA} \propto \frac{M_{ge}^2 \Delta\mu_{ge}^2}{\Gamma} \quad (1)$$

where M_{ge} and $\Delta\mu_{ge}$ are the transition dipole moment and the change in the dipole moment from ground to excited states, respectively; and Γ is the damping factor. It is important to note that the TPA cross-section (δ_{TPA}) value is strongly

[a] Beijing National Laboratory for Molecular Sciences (BNLMS), Key Laboratory of Photochemistry, Institute of Chemistry, Chinese Academy of Sciences, Beijing 100190, People's Republic of China. E-mail: andong@iccas.ac.cn.
[b] Department of Chemistry, National University of Singapore, 3 Science Drive 3, Singapore 117543, Singapore. E-mail: chmcc@nus.edu.sg.

†Electronic Supplementary Information (ESI) available: additional details of solvent effects and spectral properties, the optical structures and molecular orbitals, decomposed transient absorption in selected time delay, kinetics at selected wavelength from transient absorption spectra. See DOI: 10.1039/x0xx00000x

depended on the values of M_{ge} and $\Delta\mu_{ge}$. To realize the direct correlation of δ_{TPA} with M_{ge} and $\Delta\mu_{ge}$, we report the comparative study of the solvent-dependent spectral properties of three tribranched donor-π-acceptor (octupolar) chromophores (DA_3) with TAT as a planar, conjugated-core. Here, **TAT-Bz**, **TAT-T-Bz** and **TAT-T-PhCN** (the molecular structures are shown in Scheme 1) were chosen for the investigation of the effect of extended conjugation with the same electron-donating but different electron-withdrawing abilities, where **TAT-Bz** and **TAT-T-Bz** have the same donor-acceptor pair but different π-bridge lengths, whereas **TAT-T-Bz** and **TAT-T-PhCN** have the same planar electron donating core and conjugated length, but different electron-withdrawing groups at the terminal sites. Since the donor-acceptor related spectral properties of multidimensional molecules are strongly depended on the surrounding environments, such as polarity of matrix or solvents, we are curious to know how much the exact environmental effect on excitation delocalization/localization in multibranched push-pull chromophores can be expected for the planar, π-conjugated octupolar molecules core.

In this work, spectral measurements and quantum chemical calculations are carried out to reveal how the multidimensioned ICT in these tribranched chromophores related to the TPA properties by estimating the TPA essential factors (M_{ge} and $\Delta\mu_{ge}$). The results of solvation effects and the dynamics of the excited states show that the excited state of these three chromophores tend to exhibit an excited localization on one of the dipolar branches, which is beneficial to achieve large M_{ge} and $\Delta\mu_{ge}$ to achieve the high TPA properties.

Scheme 1. Molecular Structures of Tribranched Chromophores.

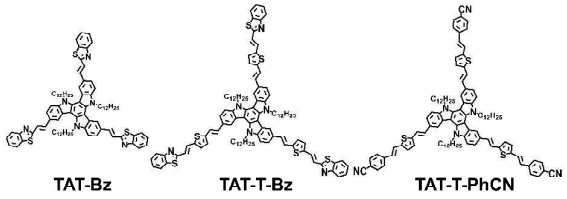

Materials and Methods

Materials

The synthesis and characterization of star-shaped octupolar TAT-based chromophores were reported previously.[17] The chemical structures and purities are identified by ^{1}H NMR, ^{13}C NMR spectroscopy, mass spectrometry, and elemental analysis. For the spectroscopic measurements, purified **TAT-Bz**, **TAT-T-Bz** and **TAT-T-PhCN** were dissolved in aprotic solvents.

Absorption and Fluorescence Measurements

UV-vis absorption spectra were carried out by a Hitachi U-3010 spectrophotometer. The steady-state fluorescence measurements were recorded on F-4600 (Hitachi) fluorescence spectrometer.

Fluorescence excitation anisotropy spectra were recorded with the same fluorescence spectrophotometer (F-4600, Hitachi) by passing the excitation and emission light through two polarizers, respectively. Experimentally, the anisotropy (r) is given by the following equation:

$$r = \frac{I_{VV} - GI_{VH}}{I_{VV} + 2GI_{VH}} \quad (2)$$

Here the two subscripts are the orientation of the excitation and emission polarizers, respectively. G ($G = I_{HV}/I_{HH}$) is the geometric factor of the fluorescence spectrometer which is easily measured by the ratio of the sensitivities of the detection system for vertically and horizontally polarized light.

Computational Details

The ground-state structure optimizations were done by density functional theory (DFT) at the B3LYP/6-31G(d,p) level as implemented in the Gaussian 09 package.[34] For the sake of simplicity, the dodecyl solubilizing groups were replaced with methyls. All optimized structures were characterized by an analytical frequency analysis and were shown to be the minima without imaginary frequencies. On the optimized ground-state structure, time-dependent DFT (TDDFT) at the same level were carried out to calculate the vertical transition from ground state to excited states. Structures and orbitals were visualized using GaussView version 5.0, which was also used to generate charge difference density contours.

Femtosecond Transient Absorption Measurements

The femtosecond transient absorption measurements with time resolution about 90 fs were conducted using a homemade femtosecond broadband pump-probe setup detecting in visible region.[35-39] For the current pump-probe measurements, every spectrum was measured using magic-angle polarizer conditions. Concentration of the tribranched chromophores was adjusted to an absorbance of ~0.3 OD at 400 nm in a 1 mm path length quartz cuvette.

The original time-resolved spectra are corrected for stray light and for the group velocity dispersion of the white light (chirp), which was done by fitting a polynomial to the cross phase modulation signal of the pure solvent under identical experimental conditions. Then data analysis was performed with the global and target analysis program Glotaran based on the statistical fitting package TIMP.[40, 41] In the case of a sequential model, each evolution-associated difference spectrum (EADS) corresponds again to one exponential decay that also constitutes the population for the subsequent decay.[42-44]

Results and Discussion

Steady Absorption Spectra and Transition Dipole Moments

Figure 1 shows the normalized UV-vis spectra of the tribranched chromophores in toluene, chloroform, tetrahydrofuran (THF) and dichloromethane (DCM), respectively. The detailed spectral parameters are presented in Table S1 (Supporting Information). Each of these chromophores exhibited two major absorption bands. The high-energy absorption bands, which are in the same region around 330 nm, correspond to the localized $\pi - \pi^*$ transition of the conjugated TAT core,[17,26,45] while the low-energy bands in the visible region result from the ICT transitions. The characters of ICT are also demonstrated from quantum-chemical calculations of the investigated tribranched compounds (see Figure S2 and Figure 5). It is found that the HOMO orbitals are delocalized over the TAT core and parts of branches, whereas the LUMO orbitals mainly located on the accepting peripheries.

Furthermore, as shown in Figure 1, the absorption spectra for each investigated chromophore in different polar solvents have no obvious changes, indicating the nearly net zero dipole moments of ground states because of rigid and planar TAT core with symmetric ground structure. However, for **TAT-Bz** and **TAT-T-Bz** with the same donor-acceptor pair but different π-bridge lengths, lengthening the π-conjugation bridges by the introduction of conjugated thienylene vinylene unit for **TAT-T-Bz** results in obvious bathochromic shifts of both ICT absorption and fluorescence, where the absorption spectra (see Figure 1a and b) show large red-shifts of absorption spectra from 400 nm for **TAT-Bz** to 450 nm for **TAT-T-Bz.** Moreover, in the case of **TAT-T-PhCN** with the same electron donating core but less strength of the electron acceptor groups relative to **TAT-T-Bz**, a slight blue-shift of absorption around 440 nm for **TAT-T-PhCN** is observed relative to the absorption around 450 nm for **TAT-T-Bz**, indicating strong electron withdrawing ability leads to the enhanced intramolecular charge transfer.

The same trends are also observed in the fluorescence spectra as shown in Figure 1, where the red-shift is less pronounced in fluorescence with different electron acceptors (**TAT-T-Bz** and **TAT-T-PhCN**), but more pronounced with different conjugated lengths (**TAT-Bz** and **TAT-T-Bz** or **TAT-T-PhCN**), indicating the large geometry-dependence changes of dipole moments of the excited states, which will be discussed in detail in the next section of "Fluorescence Spectra and Solvation Effects".

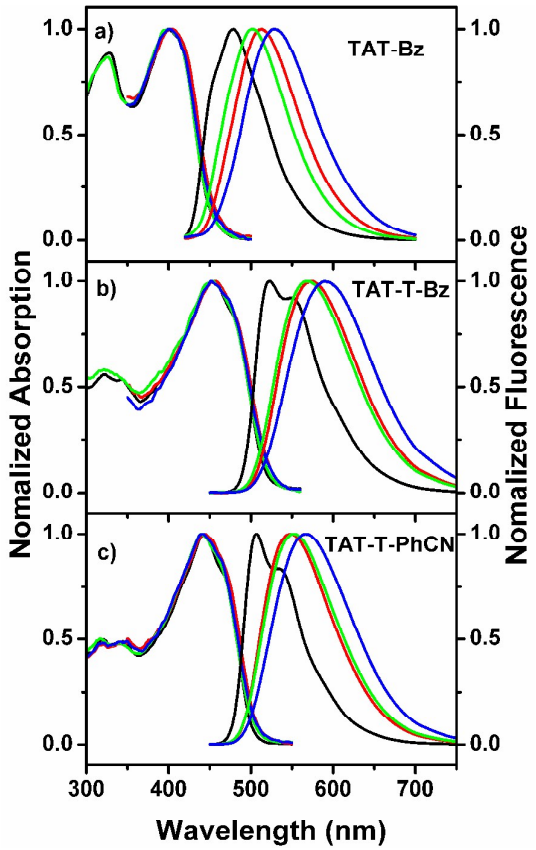

Figure 1. Normalized absorption and fluorescence spectra of **TAT-Bz** (a), **TAT-T-Bz** (b) and **TAT-T-PhCN** (c) in different solvents: toluene (black), chloroform (red), THF (green) and DCM (blue).

According to the description of equation (1),[14,32] the TPA cross-section (δ_{TPA}) of lowest-energy absorption is directly corresponding to the transition dipole moments (M_{ge}), which is an essential factor for the tribranched chromophores. To obtain the transition dipole moments (M_{ge}), we have estimated the absorption transition moments from steady-state electronic absorption measurements according to the formulas used in the literature,[33,46]

$$M_{ge} = \left[\frac{1500(\hbar c)^2 \ln 10}{\pi N_A E_{ge}} \int \varepsilon_{ge}(\nu) \mathrm{d}\nu \right]^{1/2} \quad (3)$$

where N_A is Avogadro's number, $\varepsilon_{ge}(\nu)$ is the extinction coefficient (in $M^{-1} \cdot cm^{-1}$) at the wavenumber ν , in cm^{-1} , and the integral is performed over the first absorption band. Table 1 list the corresponding parameters about steady-state absorption and transition dipole moments (M_{ge}) as well as two-photon absorption cross sections of the investigated chromophores in THF. It is found that, those chromophores with larger conjugation and stronger electron-withdrawing ability show better performance in the TPA cross sections because of larger M_{ge} .

Table 1. Photophysical parameters of the investigated chromophores in THF

	λ_{abs}(nm)[a]	ε($cm^{-1} \cdot M^{-1}$)[a]	M_{ge}(D)[b]	$\Delta\mu_{ge}$(D)[c]	δ_{TPA}(GM)[d]
TAT-Bz	400	86000	12.1	19.0	1110
TAT-T-Bz	454	142700	17.8	23.9	1600
TAT-T-PhCN	441	133000	16.4	23.1	1410

a. λ_{abs} and ε are the absorption peak and molecular extinction coefficient. The results are consistent with the previous report. b. M_{ge} is the transition dipole moments obtained by the equation (3). Errors in the determined M_{ge} are about 10%. c. $\Delta\mu_{ge}$ is obtained from Lippert-Mataga relationship. d. δ_{TPA} is from our previous work.[17]

Fluorescence Spectra and Solvation Effects

As shown in Figure 1, the red-shift of fluorescence is less pronounced for those chromophores with different electron acceptors but more pronounced with different conjugated length, this could lead to large correlation with excited state dipole moments. According to the aforementioned equation (1), the TPA cross-section (δ_{TPA}) for the TPA compounds is also dependent on the change ($\Delta\mu_{ge}$) in the dipole moment between the excited and ground state. To estimate $\Delta\mu_{ge}$, the solvation effects are further conducted for these three compounds. As discussed above, there is no obvious solvatochromism for these compounds in different polar solvents observed from absorption spectra because of the C_3 symmetry which leads to nearly net zero permanent dipole moment of ground state. In contrast to less shifted absorption spectra, the fluorescence spectra are much sensitive to the solvent polarity. When the

solvent was changed from non-polar cyclohexane to polar acetone (i.e. with an increase in the polarity of solvents), as shown in Figure 1 and Table S1, the fluorescence maxima shifts from 460 nm to 534 nm for **TAT-Bz**, from 504 nm to 598 nm for **TAT-T-Bz** and from 492 nm to 581 nm for **TAT-T-PhCN**, respectively. This further proves the strong ICT from electron-donor core to electron-acceptor peripheries, indicating the polar nature of the excited states of these chromophores. The ICT effect facilitates good electronic communication functionality and contributes to the red-shifted fluorescence spectra of chromophores upon solvation. In Figure 2, the absorption and fluorescence peaks of **TAT-Bz**, **TAT-T-Bz** and **TAT-T-PhCN** are plotted as a function of the polarity of different solvents (from cyclohexane to acetone, in the form of Reichardt parameters).[47] These plots are clearly demonstrated that solvent-induced red-shift is pronounced in fluorescence spectra than in absorption spectra.

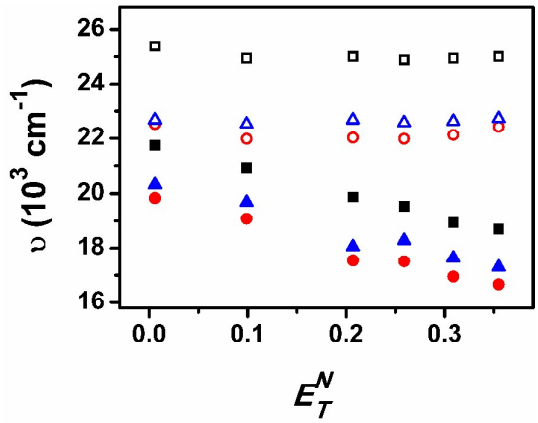

Figure 2. Absorption (open) and fluorescence (filled) band peaks as a function of solvent polarity. Squares, **TAT-Bz**; circles, **TAT-T-Bz**; triangle, **TAT-T-PhCN**.

In order to estimate the dipole moment difference ($\Delta\mu_{ge}$) between the excited- and ground-state dipole moments, we employed an alternative method by Lippert and Mataga to correlate the Stokes shift with the orientational polarizability of each solvent to further determine the solvent effects on the polar nature of the excited states of these chromophores.[48,49] The fact that both solvent-independent absorption spectra and solvent-dependent fluorescence spectra strongly indicate that the excited state of these tribranched compounds could dramatically enter a strongly polar excited ICT state from the initial Franck-Condon state. The relationship between Stokes shift and the polarity of solvent can be simply described by the Lippert-Mataga equation[49-51]

$$\Delta\upsilon = \upsilon_{abs} - \upsilon_{em} = \frac{2\Delta f}{hca^3}\left(\Delta\mu_{ge}\right)^2 + const \qquad (4)$$

where, $\Delta\upsilon$ is the Stokes shift, υ_{abs} and υ_{em} are the absorption and emission energy in wavenumber, respectively and h is the Planck constant, c is the light speed, a is the Onsager cavity radius[52], $\Delta\mu_{ge}$ ($\Delta\mu_{ge} = \mu_e - \mu_g$) is the difference between the excited- and ground-state dipole moments. Δf , known as the solvent polarizability, which can be captured using the dielectric constants (ε) and refractive indices (n) of the solvents by the following equation:

$$\Delta f = \frac{(\varepsilon - 1)}{(2\varepsilon + 1)} - \frac{(n^2 - 1)}{(2n^2 + 1)} \qquad (5)$$

Figure 3 shows the plots of $\Delta\upsilon$ versus Δf for three chromophores. Linear regression fits yield $2\Delta\mu_{ge}^2 / hca^3$ from the slope, which is the key output from the Lippert-Mataga analysis. The slopes of **TAT-T-Bz** and **TAT-T-PhCN** are nearly identical but larger than that of **TAT-Bz,** indicating that the conjugated length has the stronger impact on polar degree of ICT relative to the electron accepting ability. The good and linear fit of Lippert-Mataga plots suggests that the emitting state most likely arise from the charge localization on one branch.[11,16] To quantitatively determine the polarity of the ICT state, we examined the dipole moment change ($\Delta\mu_{ge}$) between the excited-state and ground-state based on the equations (4) and (5). We use the Onsager cavity radius (7.30 Å for **TAT-Bz**, 8.09 Å for **TAT-T-Bz** and 7.97 Å for **TAT-T-PhCN**) to calculate the effective dipole moment changes, which are 19.0 D, 23.9 D, 23.1 D for **TAT-Bz**, **TAT-T-Bz** and **TAT-T-PhCN**, respectively. Here, the Onsager cavity radius (a) is estimated from the quantum-chemical calculations using density functional theory method at the B3LYP/6-31G(d,p) level. Compared to **TAT-T-Bz** and **TAT-T-PhCN** with longer conjugation, as shown above, $\Delta\mu_{ge}$ of **TAT-Bz** (19.0 D) is a little smaller, which could be attributed to the shorter conjugation. The deduced $\Delta\mu_{ge}$ values from Lippert-Mataga analysis for these compounds are in agreement with the observed TPA cross sections as shown in Table 1. Particularly, since the dipole moments in ground states are nearly zero for all these three compounds, the fact that no obvious shifts of absorption but large much more red-shift of the fluorescence spectra in various solvents are observed, indicating that the obtained dipole moment changes are almost contributed from the excited states. Such a positive solvatochromism was commonly observed for many push-pull chromophores due to intrinsic C_3-symmetral ground states and photoinduced ICT from the planar core to the periphery, leading to the ICT localization on one arm of the emitting state, especially for the those push-pull chromophores with long conjugation like **TAT-T-Bz** and **TAT-T-PhCN**[14,53,54] because of symmetry-broken excited states upon excitation.

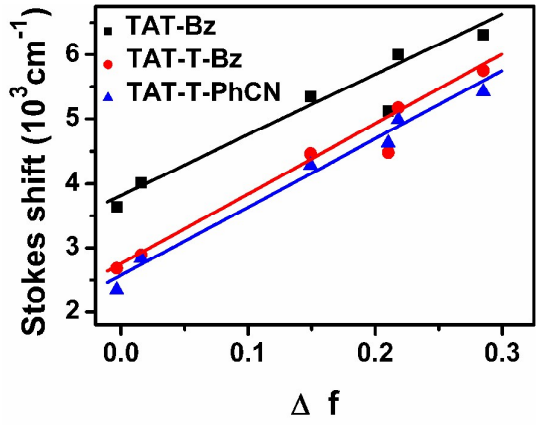

Figure 3. Lippert-Mataga plots showing the Stokes shift versus the solvent polarity function for tribranched chromophores **TAT-Bz** (black), **TAT-T-Bz** (red) and **TAT-T-PhCN** (blue), respectively. Solid lines are the fitted results.

Fluorescence Excitation Anisotropy Spectra

To estimate the nature of localized emission and symmetry-broken excited state upon excitation in the investigated chromophores with 3-fold symmetry, we performed steady-state fluorescence excitation anisotropy measurements on the tribranched molecules.[14,39] In order to avoid the rotation of molecules during excited state relaxation, all the investigated compounds are doped in an isotropic polystyrene film. Figure 4 shows the fluorescence excitation spectra and fluorescence excitation anisotropy spectra of these chromophores. The excitation spectra were measured by monitoring the red-side of fluorescence at 510, 570 and 550 nm for **TAT-Bz**, **TAT-T-Bz** and **TAT-T-PhCN**, respectively. The redistribution of the excitation energy among the three spatial transition dipoles lead to the limiting anisotropy should reach 0.1 for these tribranched chromophores.[39,54,55] It is found that the anisotropy of these three chromophores follows the similar trends. The anisotropy is around 0.1 at the higher energy side, and gradually increases with the decreased excitation energy at the low energy region, and then reaches an anisotropy limit around 0.4. Without rotation, this anisotropy changes could be explained by an energy transfer mechanism among three branches with these chromophores, indicating that the localized excited state in one of the three branches is generated because of symmetry-broken excited state upon excitation.[14,39,56] The excited states of each branch can be excited by different excitation wavelength in the ICT region, where the exergonic energy transfer result in an anisotropy decrease of the high-energy ICT state. The energy transfer with excitation at the lower energy side, an endergonic process to other branches, is less effective. As a result, the anisotropy is expected to be ~0.4 at the low-energy side. To gain deeper insight to the nature of ICT state, the following charge difference density (CDD) calculations were carried out, where CDD means the difference in electron density upon vertical transition between ground state and excited states.

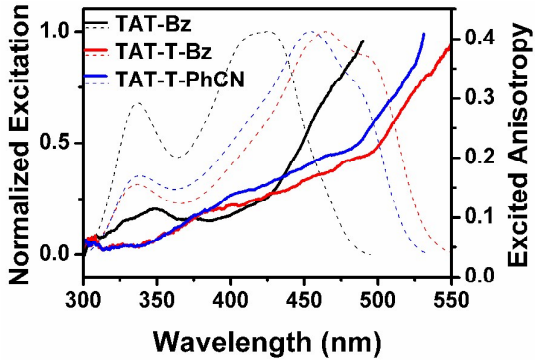

Figure 4. Fluorescence excitation anisotropy spectra (solid lines) and normalized fluorescence excitation spectra (dashed lines) of chromophores **TAT-Bz**, **TAT-T-Bz** and **TAT-T-PhCN** in an isotropic polystyrene film at room temperature.

Computation Studies

Geometrical optimization calculations were performed with B3LYP/6-31G(d,p) level of theory for these three tribranched chromophores in the ground state. The discotic structures along C_3-symmentry (shown in Figure S2) were obtained by optimization without imaginary frequencies. The optimized structures reveal that the substituted electron-withdrawing groups attached to the ends of chromophores are nearly coplanar with the TAT backbone. Thus, the delocalization between the arms cannot be ignored in ground states. However, the optimized lowest excited states (by TDDFT method) do not retain their symmetries. The dipole moment of ground state is almost zero, while that of the lowest excited state is very large. The planar structure of chromophores is beneficial to enhance the TPA cross section. Upon excitation, charge localization on one branch is better for obtaining a strong dipolar excited state.

The relative ordering of frontier molecular orbitals could provide a reasonable qualitative indication of the excited state properties. The contour plots of important frontier molecular orbitals of the three chromophores are shown in Figure S2. To clearly verify the charge transfer pathway in the three compounds, the visualized charge difference density (CDD) based on TDDFT methods at the same level were performed. Figure 5 shows the visualized CDDs of $S_1 - S_0$ transition, presenting direct evidence of intramolecular charge transfer from the inner core to the peripheral groups, where the triazatruxene core acts as electron-donor and benzothiazol or 4-cyanophenyl moieties act as electron acceptor. As shown in Figure 5 the CDD of **TAT-Bz** still maintains C_3-symmentry to some extent because of the planar core which keeps the structural rigidity with the acceptor via short π-conjugated bridge, whereas the CDDs of **TAT-T-Bz** and **TAT-T-PhCN** show clearly localization because of longer conjugated bridge between donor and acceptor groups. As mentioned above, the nature and the charge transfer degrees of the ICT states are strongly influenced by the polarity of the surrounding solvents, where the larger the dipole moment changes ($\Delta\mu_{ge}$) in the excited state are, the stronger the solvation is. Femtosecond transient absorption measurements can thus provide more insight about the correlation of solvation with the dipole moment changes ($\Delta\mu_{ge}$) between the ground and the excited states by determining the solvent-dependent dynamics of the excited ICT states.

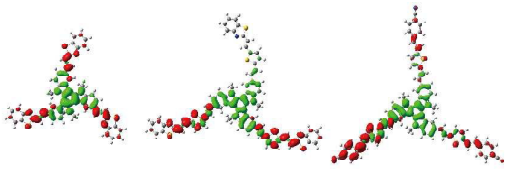

Figure 5. Density difference between the lowest charge-transfer and ground states of chromophores. From left to right, the molecule is **TAT-Bz**, **TAT-T-Bz** and **TAT-T-PhCN**, respectively. The green and red represent the hole and electron, respectively.

Transient Absorption Spectroscopy

For a detailed understanding of the excitation delocalization, charge localization, and the polar nature of ICT state in these TAT derivatives, femtosecond transient absorption measurements have been carried out to provide more insight about the correlation of solvation with the dipole moment changes ($\Delta\mu_{ge}$). The samples were excited at 400 nm, and the resulting absorbance differences were recorded in a visible spectral region between 425 nm and 780 nm. Since without specific solute-solvent interaction (such as H-bond dynamics, which may cause an extra dynamics in the observed spectra[57]), the dynamics of aprotic solvents reorganization around the excited solute molecule is mainly determined by solvent polarity and the polar dipole moment of excited solute molecules. Here in THF, a medium polar solvent as an example, the dynamics of these three investigated chromophores are associated with the polar degree of the excited state, which is an essential factor to the photophysical properties. The transient absorption spectra at different time

delays from 300 fs to 20 ps and a long delay time (500 ps) for **TAT-Bz**, **TAT-T-Bz** and **TAT-T-PhCN** in THF are shown in Figure 6. According to steady absorption and fluorescence spectra as shown in Figure 1, the ground state bleaching (GSB) and stimulated emission (SE) over the whole spectral region, are corresponding to the positions of absorption and fluorescence, respectively. For **TAT-Bz**, there is a strong, board excited states absorption (ESA, positive absorption signal) from 500 to 780 nm and a weak ESA (at around 450 nm) with the negative GSB and SE band, which seems below zero. The shapes of transient spectra of the extended π-conjugation systems (**TAT-T-Bz** and **TAT-T-PhCN**) are similar, but very different from that of **TAT-Bz**. For **TAT-T-Bz** and **TAT-T-PhCN**, GSB and SE are slight shift to the longer wavelength because of the more extending conjugation. There are two ESA peaks, where the decay of the strong ESA located above 700 nm occurs together with the increase of the weak one between 500 nm and 550 nm. This process may correspond to the solvation-dependent structural relaxation.[16,21,33,39,54] It has been reported for the TPA tribranched chromophores that the relaxation from the initially populated Franck-Condon state to the charge-localized ICT state happened much fast in several hundred femtoseconds.[16,21,39] Then the polar ICT state shows pronounced solvation in sequential decay.

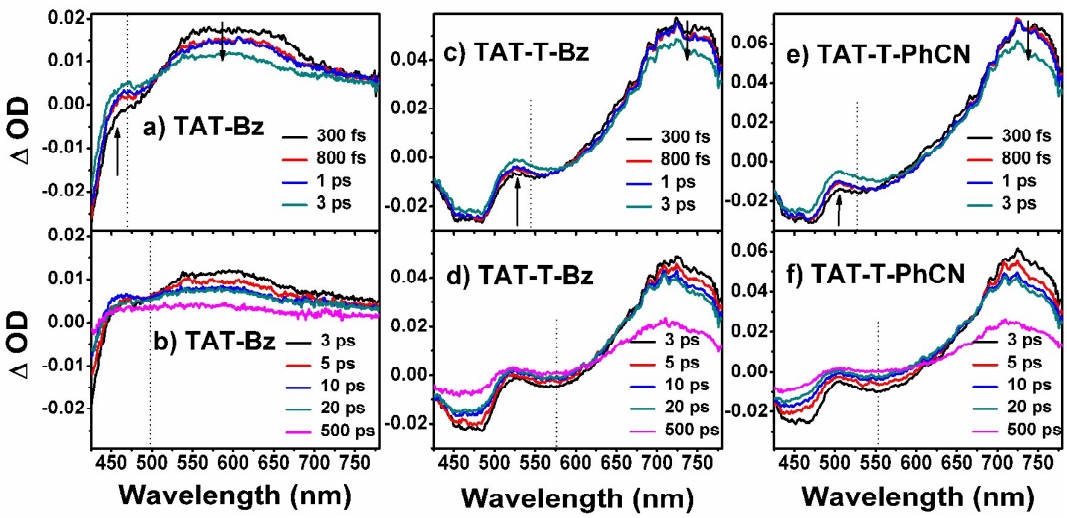

Figure 6. Evolution of femtosecond transient absorption spectra. The spectral evolution is separated in two time domain 300 fs -3 ps (top), 3-20 ps and 500 ps (bottom). The dashed lines in each panel are guides to the eye for identifying the red-shift of SE peak.

As shown in top panels of Figure 6(a, c, e), the vertical dashed lines were positioned at the wavelength of the initial SE bands (around 300 fs). It is obviously found that the transient spectra of these chromophores mainly consists of a red shift of the SE band in the first few picoseconds. Noticeably, for each compound, the shape of spectra from 5 ps to 20 ps is almost same, which means that the solvation process is over. In order to estimate the excited state deactivation, the dynamic Stokes shift is extracted from the corresponding transient absorption spectra by decomposing the transient absorption spectra with Gaussian peaks[39,58-61] (see Figure S3, Supporting Information). The time dependent peak shift from the position at 0.2 ps can thus be calculated from the Gaussian peak at different delay times. The results are shown in Figure 7(a). Relaxation functions for these tribranched chromophores are compared in Figure 7(b), where normalized values $C(t) = (\nu(t) - \nu(\infty)) / (\nu(200\,fs) - \nu(\infty))$ are shown.[62] The exponential fitting parameters of relaxation dynamics are shown in Table 2.

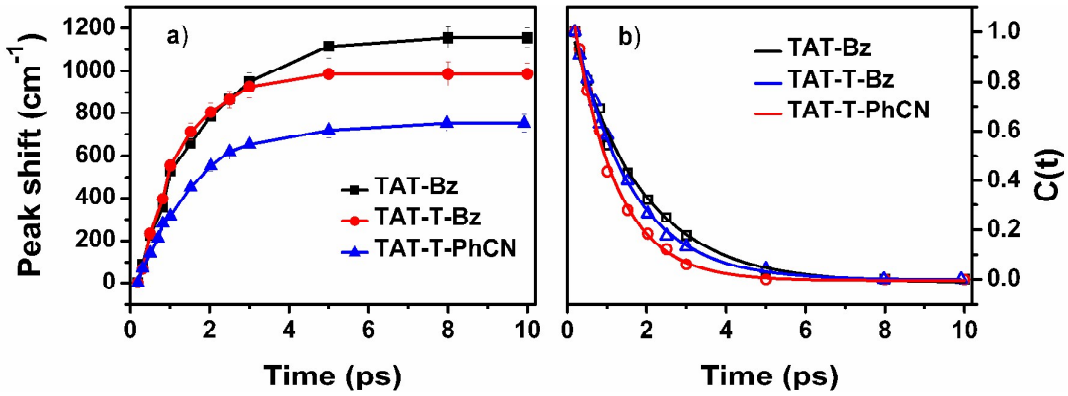

Figure 7. (a) Peak shift dynamics; (b) peak-frequency relaxation, normalized to 1 at t = 200 fs and 0 at long delay time while solvation ended, respectively.

Table 2. Summary of the solvation time deduced from the red-shift of SE band and global lifetimes of excited states of tribranched chromophores in THF

	Solvation time	Lifetimes by global fitting		
	τ (ps)	τ_1 (fs)	τ_2 (ps)	τ_3 (ps)
TAT-Bz	1.75 ± 0.15	450 ± 20	5.6 ± 0.6	~ 910
TAT-T-Bz	1.05 ± 0.1	465 ± 30	4.5 ± 0.3	~ 900
TAT-T-PhCN	1.42 ± 0.1	460 ± 20	5.0 ± 0.5	~ 840

Furthermore, a clear isobestic point is observed with the evolution of the transient spectra, indicating a new transient in the region around 500 nm formed with a decay of ESA at the red region. This is a solvent stabilized ICT state (ICT') conformationally from the initial excited states as reported in many similar push-pull molecules before.[16,21,33,39] The dynamic evolution of the three chromophores are further better visualized by inspecting the evolution associated difference spectra (EADS) obtained by global analysis, using a sequential kinetics scheme with increasing lifetime.[40,41] The good quality of the fit is testified by a very low value of the root-mean-square error (RMS), which is less than 0.001, and the results of fitting were shown in Figure 8 and Table 2. A fast vibrational relaxation from Franck-Condon state takes place in a few hundred femtoseconds. Then the vibrationally relaxed ICT state decays with a lifetime of several picoseconds to yield a final relaxed ICT state. Finally, the stabilized ICT state decays with a lifetime of around one nanosecond, which is close to the lifetime of fluorescence.[16,21,33,39]

It can be seen in Table 2 that the solvation time constants (~1 ps) are consistent with the previous reports, indicating that the localization of the excited state of tribranched chromophores.[35,60] The observed solvation times about 1.05 ps and 1.42 ps are faster in the case of **TAT-T-Bz** and **TAT-T-PhCN** when compared to **TAT-Bz** (1.75 ps) in the same polar solvent, which is related to $\Delta\mu_{ge}$ upon excitation. Since the nearly net zero dipole moments of ground states for all these three compounds because of rigid and planar TAT core with symmetric ground structure as mentioned above, the initial excited ICT state could be a dipole and as the long conjugation **TAT-T-Bz** and **TAT-T-PhCN** is much more polar than **TAT-Bz.** In such a case, the dipole moment of the excited states would be the main contributing factor for $\Delta\mu_{ge}$. Therefore, the formation of the solvent-stabilized ICT state is mainly influenced by the degree of polar excited state. The fitted time constants of τ_2 reflects the solute-solvent interaction of the investigated system. For the same polar solvent, the time constants mainly depend on $\Delta\mu_{ge}$, this is all contributed from the dipolar excited states becasue of nearly net zero dipole moments of ground states for all these three compounds. Thus the results of femtosecond transient absorption agree well with the estimation of $\Delta\mu_{ge}$ by Lippert-Mataga relationship mentioned above. Typically, the solvation for **TAT-T-Bz** is faster compared to **TAT-Bz**, indicating that extended conjugation by introduction of thienylene vinylene is an efficient method to obtain high $\Delta\mu_{ge}$ and to enhance the TPA properties. As mentioned in the equation (1), several parameters determine the TPA cross section of molecules. Based on the sum-over-states method, both M_{ge} (obtained by the steady state absorption) and $\Delta\mu_{ge}$ (obtained by the solvation of the excited state) are the essential factors of the TPA cross section, thus the rigid and planar structures of the TAT core could be a good alternative by improving higher M_{ge} and $\Delta\mu_{ge}$ to achieve the higher TPA properties compared with the twist structures.[16,21]

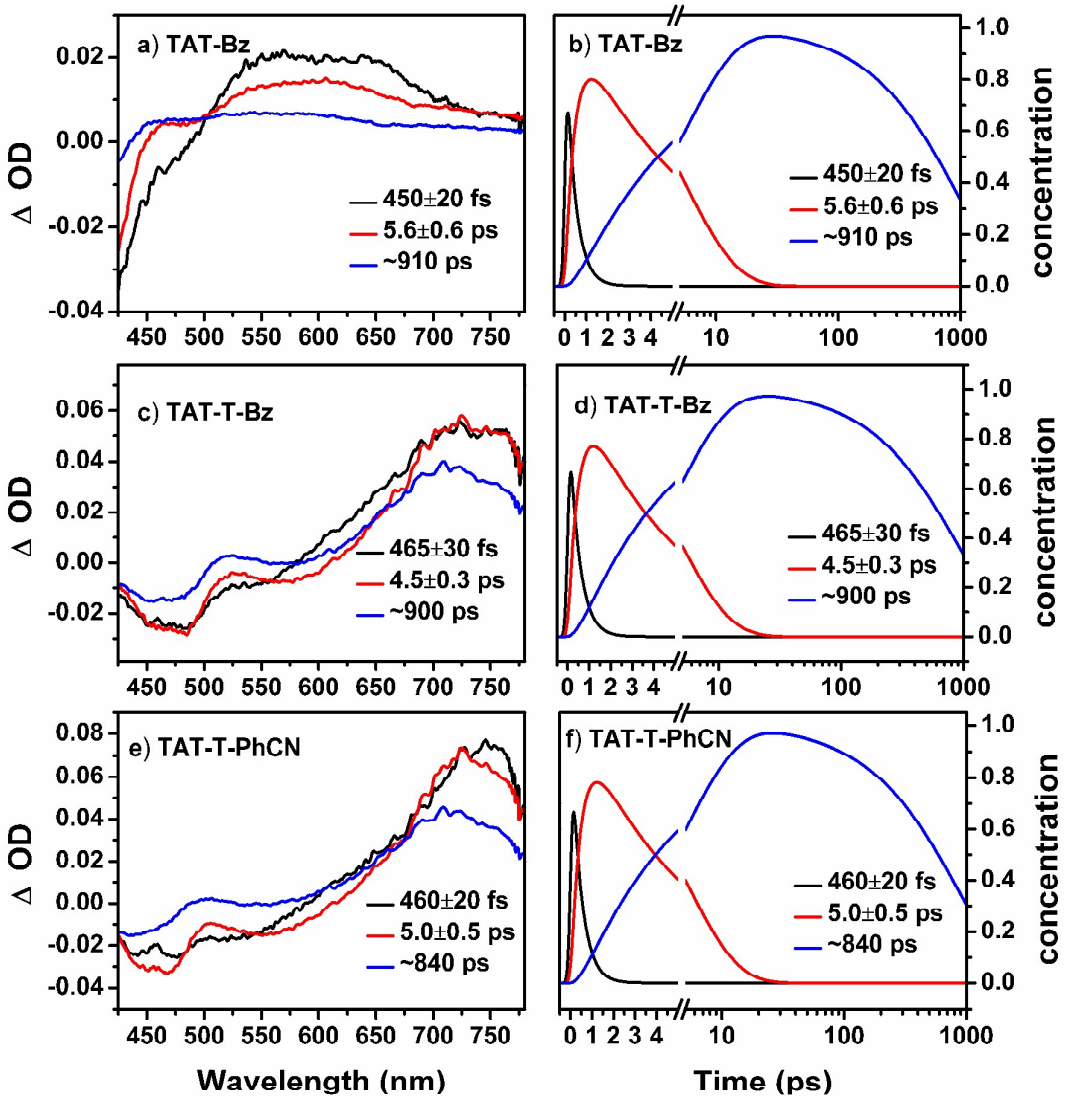

Figure 8. Global analysis of the transient absorption spectra. EADS obtained using a sequential relaxation model for **TAT-Bz** (a), **TAT-T-Bz** (c) and **TAT-T-PhCN** (e) in THF. The associated population evolution curve of the EADS components as a function of time for **TAT-Bz** (b), **TAT-T-Bz** (d) and **TAT-T-PhCN** (f). Kinetics at selected wavelengths for showing the good quality of global fitting for chromophores in Figure S4-S6.

Conclusions

In summary, the multidimensioned ICT properties of three organic octupolar chromophores containing planar TAT as the central electron donor with different electron-withdrawing groups at the terminal sites, have been comparatively investigated in order to understand the structure-properties relationship of electronic push-pull chromophores. The transition dipole moments (M_{ge}) and the change of dipole moments ($\Delta\mu_{ge}$) between ground and excited states, which are essential factors for TPA properties, were determined by steady state spectra, transient absorption measurements and quantum chemical calculations. It is found that the intramolecular charge transfer in the excited states plays an important role in improving the TPA properties. As results that for the electron donor-acceptor system, the strategies by introduction of thienylene vinylene to enhance the TAT donor ability and modifying the strength of the electron-withdrawing-groups as well as the length of the conjugation, are possible to increase the TPA cross section (δ_{TPA}). Following the same trends of M_{ge} and $\Delta\mu_{ge}$, **TAT-T-Bz** and **TAT-T-PhCN** exhibit larger TPA cross section than **TAT-Bz** because of the extended conjugation. This current work provides deeper understanding of the correlation between the TPA properties and the octupolar molecular structures, which could be helpful to the judicious design of the star-shaped compounds with better photophysical properties.

Acknowledgements

This work was supported by the 973 Program (No. 2013CB834604), NSFCs (Nos. 21173235, 91233107, 21127003, 21333012, and 21373232) and the Strategic Priority

Research Program of the Chinese Academy of Sciences (Grant No.XDB12020200). C. C. acknowledges the financial support from MOE Tier 1 grant (R-143-000-573-112).

References

1. P. L. Burn, S. C. Lo and I. D. W. Samuel, *Adv. Mater.*, 2007, **19**, 1675-1688.
2. B. O'Regan and M. Grätzel, *Nature*, 1991, **353**, 737-740.
3. J. Roncali, *Chem. Rev.*, 1997, **97**, 173-206.
4. S.-C. Lo and P. L. Burn, *Chem. Rev.*, 2007, **107**, 1097-1116.
5. D. Collado, P. Remón, Y. Vida, F. Najera, P. Sen, U. Pischel and E. Perez-Inestrosa, *Chem. Asian J.*, 2014, **9**, 797-804.
6. S. Yao, H.-Y. Ahn, X. Wang, J. Fu, E. W. Van Stryland, D. J. Hagan and K. D. Belfield, *J. Org. Chem.*, 2010, **75**, 3965-3974.
7. J. C. Collings, S.-Y. Poon, C. Le Droumaguet, M. Charlot, C. Katan, L.-O. Pålsson, A. Beeby, J. A. Mosely, H. M. Kaiser, D. Kaufmann, W.-Y. Wong, M. Blanchard-Desce and T. B. Marder, *Chemistry – A European Journal*, 2009, **15**, 198-208.
8. A. Cravino, P. Leriche, O. Alévêque, S. Roquet and J. Roncali, *Adv. Mater.*, 2006, **18**, 3033-3037.
9. A. M. McDonagh, M. G. Humphrey, M. Samoc, B. Luther-Davies, S. Houbrechts, T. Wada, H. Sasabe and A. Persoons, *J. Am. Chem. Soc.*, 1999, **121**, 1405-1406.
10. K. Sénéchal, O. Maury, H. Le Bozec, I. Ledoux and J. Zyss, *J. Am. Chem. Soc.*, 2002, **124**, 4560-4561.
11. C. Katan, F. Terenziani, O. Mongin, M. H. V. Werts, L. Porrès, T. Pons, J. Mertz, S. Tretiak and M. Blanchard-Desce, *J. Phys. Chem. A*, 2005, **109**, 3024-3037.
12. C. K. Wang, P. Macak, Y. Luo and H. Agren, *J. Chem. Phys.*, 2001, **114**, 9813-9820.
13. P. Macak, Y. Luo, P. Norman and H. Agren, *J. Chem. Phys.*, 2000, **113**, 7055-7061.
14. L. Yan, X. Chen, Q. He, Y. Wang, X. Wang, Q. Guo, F. Bai, A. Xia, D. Aumiler, S. Vdović and S. Lin, *J. Phys. Chem. A*, 2012, **116**, 8693-8705.
15. Y. Wan, L. Yan, Z. Zhao, X. Ma, Q. Guo, M. Jia, P. Lu, G. Ramos-Ortiz, J. L. Maldonado, M. Rodríguez and A. Xia, *J. Phys. Chem. B*, 2010, **114**, 11737-11745.
16. G. Ramakrishna and T. Goodson, *J. Phys. Chem. A*, 2007, **111**, 993-1000.
17. J. Shao, Z. Guan, Y. Yan, C. Jiao, Q.-H. Xu and C. Chi, *J. Org. Chem.*, 2011, **76**, 780-790.
18. G. Wu, G. Zhao, C. He, J. Zhang, Q. He, X. Chen and Y. Li, *Sol. Energy Mater. Sol. Cells*, 2009, **93**, 108-113.
19. P. C. Ray and J. Leszczynski, *J. Phys. Chem. A*, 2005, **109**, 6689-6696.
20. M. Velusamy, J.-Y. Shen, J. T. Lin, Y.-C. Lin, C.-C. Hsieh, C.-H. Lai, C.-W. Lai, M.-L. Ho, Y.-C. Chen, P.-T. Chou and J.-K. Hsiao, *Adv. Funct. Mater.*, 2009, **19**, 2388-2397.
21. A. Bhaskar, G. Ramakrishna, Z. Lu, R. Twieg, J. M. Hales, D. J. Hagan, E. Van Stryland and T. Goodson, *J. Am. Chem. Soc.*, 2006, **128**, 11840-11849.
22. P. Chen, A. S. Marshall, S.-H. Chi, X. Yin, J. W. Perry and F. Jäkle, *Chem. Eur. J.*, 2015, **21**, 18237-18247.
23. X. Gan, Y. Wang, X. Ge, W. Li, X. Zhang, W. Zhu, H. Zhou, J. Wu and Y. Tian, *Dyes.Pigm.*, 2015, **120**, 65-73.
24. T. Bura, N. Leclerc, S. Fall, P. Lévêque, T. Heiser and R. Ziessel, *Org. Lett.*, 2011, **13**, 6030-6033.
25. S.-J. Chung, K.-S. Kim, T.-C. Lin, G. S. He, J. Swiatkiewicz and P. N. Prasad, *J. Phys. Chem. B*, 1999, **103**, 10741-10745.
26. Q. Ye, J. Chang, J. Shao and C. Chi, *J. Mater. Chem.*, 2012, **22**, 13180-13186.
27. J. Luo, M. Xu, R. Li, K.-W. Huang, C. Jiang, Q. Qi, W. Zeng, J. Zhang, C. Chi, P. Wang and J. Wu, *J. Am. Chem. Soc.*, 2014, **136**, 265-272.
28. E. Andrikaityte, J. Simokaitiene, A. Tomkeviciene, J. V. Grazulevicius and V. Jankauskas, *Mol. Cryst. Liq. Cryst.*, 2014, **590**, 121-129.
29. T. Bura, N. Leclerc, S. Fall, P. Leveque, T. Heiser and R. Ziessel, *Org. Lett.*, 2011, **13**, 6030-6033.
30. W. Y. Lai, Q. Q. Chen, Q. Y. He, Q. L. Fan and W. Huang, *Chem. Commun.*, 2006, DOI: 10.1039/b517841j, 1959-1961.
31. W. Y. Lai, Q. Y. He, R. Zhu, Q. Q. Chen and W. Huang, *Adv. Funct. Mater.*, 2008, **18**, 265-276.
32. D. Beljonne, W. Wenseleers, E. Zojer, Z. Shuai, H. Vogel, S. J. K. Pond, J. W. Perry, S. R. Marder and J. L. Brédas, *Adv. Funct. Mater.*, 2002, **12**, 631-641.
33. G. Ramakrishna, A. Bhaskar and T. Goodson, *J. Phys. Chem. B*, 2006, **110**, 20872-20878.
34. M. J. Frisch, G. W. Trucks, H. B. Schlegel, G. E. Scuseria, M. A. Robb, J. R. Cheeseman, G. Scalmani, V. Barone, B. Mennucci, G. A. Petersson, H. Nakatsuji, M. Caricato, X. Li, H. P. Hratchian, A. F. Izmaylov, J. Bloino, G. Zheng, J. L. Sonnenberg, M. Hada, M. Ehara, K. Toyota, R. Fukuda, J. Hasegawa, M. Ishida, T. Nakajima, Y. Honda, O. Kitao, H. Nakai, T. Vreven, J. Montgomery, J. A.;, J. E. Peralta, F. Ogliaro, M. Bearpark, J. J. Heyd, E. Brothers, K. N. Kudin, V. N. Staroverov, R. Kobayashi, J. Normand, K. Raghavachari, A. Rendell, J. C. Burant, S. S. Iyengar, M. C. J. Tomasi, N. Rega, N. J. Millam, M. Klene, J. E. Knox, J. B. Cross, V. Bakken, C. Adamo, J. Jaramillo, R. Gomperts, R. E. Stratmann, O. Yazyev, A. J. Austin, R. Cammi, C. Pomelli, J. W. Ochterski, R. L. Martin, K. Morokuma, V. G. Zakrzewski, G. A. Voth, P. Salvador, J. J. Dannenberg, S. Dapprich, A. D. Daniels, O. Farkas, J. B. Foresman, J. V. Ortiz, J. Cioslowski and D. J. Fox, *Gaussian 09 (Revision A.2)*, 2009, **Gaussian, Inc., Wallingford CT**.
35. S. Vdović, Y. Wang, B. Li, M. Qiu, X. Wang, Q. Guo and A. Xia, *Phys. Chem. Chem. Phys.*, 2013, **15**, 20026-20036.
36. M. Zhou, S. Vdović, S. Long, M. Zhu, L. Yan, Y. Wang, Y. Niu, X. Wang, Q. Guo, R. Jin and A. Xia, *J. Phys. Chem. A*, 2013, **117**, 10294-10303.
37. S. Long, M. Zhou, K. Tang, X.-L. Zeng, Y. Niu, Q. Guo, K.-H. Zhao and A. Xia, *Phys. Chem. Chem. Phys.*, 2015, **17**, 13387-13396.
38. J. Hu, Y. Li, H. Zhu, S. Qiu, G. He, X. Zhu and A. Xia, *Chemphyschem*, 2015, **16**, 2357-2365.
39. Y. Li, M. Zhou, Y. L. Niu, Q. J. Guo and A. D. Xia, *J. Chem. Phys.*, 2015, **143**.
40. J. J. Snellenburg, S. P. Laptenok, R. Seger, K. M. Mullen and I. H. M. van Stokkum, *Journal of Statistical Software*, 2012, **49**, 1-22.
41. I. H. M. van Stokkum, D. S. Larsen and R. van Grondelle, *Biochim. Biophys. Acta*, 2004, **1657**, 82-104.
42. S.-H. Lee, C. T.-L. Chan, K. M.-C. Wong, W. H. Lam, W.-M. Kwok and V. W.-W. Yam, *J. Am. Chem. Soc.*, 2014, **136**, 10041-10052.
43. M. Maiuri, J. J. Snellenburg, I. H. M. van Stokkum, S. Pillai, K. WongCarter, D. Gust, T. A. Moore, A. L. Moore, R. van Grondelle, G. Cerullo and D. Polli, *J. Phys. Chem. B*, 2013, **117**, 14183-14190.
44. C. Hippius, I. H. M. van Stokkum, E. Zangrando, R. M. Williams and F. Würthner, *J. Phys. Chem. C*, 2007, **111**, 13988-13996.
45. X. Qian, Y.-Z. Zhu, J. Song, X.-P. Gao and J.-Y. Zheng, *Org. Lett.*, 2013, **15**, 6034-6037.
46. M. Rumi, J. E. Ehrlich, A. A. Heikal, J. W. Perry, S. Barlow, Z. Y. Hu, D. McCord-Maughon, T. C. Parker, H. Rockel, S. Thayumanavan, S. R. Marder, D. Beljonne and J. L. Bredas, *J. Am. Chem. Soc.*, 2000, **122**, 9500-9510.
47. C. Reichardt, *Chem. Rev.*, 1994, **94**, 2319-2358.
48. N. Mataga, Y. Kaifu and M. Koizumi, *Bull. Chem. Soc. Jpn.*, 1955, **28**, 690-691.
49. N. Mataga, Y. Kaifu and M. Koizumi, *Bull. Chem. Soc. Jpn.*, 1956, **29**, 465-470.
50. E. Lippert, *Zeitschrift für Elektrochemie, Berichte der Bunsengesellschaft für physikalische Chemie*, 1957, **61**, 962-975.
51. N. Mataga, *Bull. Chem. Soc. Jpn.*, 1963, **36**, 654-662.

52. L. Onsager, *J. Am. Chem. Soc.*, 1936, **58**, 1486-1493.
53. C. Katan, S. Tretiak, M. H. V. Werts, A. J. Bain, R. J. Marsh, N. Leonczek, N. Nicolaou, E. Badaeva, O. Mongin and M. Blanchard-Desce, *J. Phys. Chem. B*, 2007, **111**, 9468-9483.
54. M. Jia, X. Ma, L. Yan, H. Wang, Q. Guo, X. Wang, Y. Wang, X. Zhan and A. Xia, *J. Phys. Chem. A*, 2010, **114**, 7345-7352.
55. L. Latterini, G. De Belder, G. Schweitzer, M. Van der Auweraer and F. C. De Schryver, *Chem. Phys. Lett.*, 1998, **295**, 11-16.
56. W. Verbouwe, M. Van der Auweraer, F. C. De Schryver, J. J. Piet and J. M. Warman, *J. Am. Chem. Soc.*, 1998, **120**, 1319-1324.
57. B. Bangar Raju and S. M. B. Costa, *Phys. Chem. Chem. Phys.*, 1999, **1**, 3539-3547.
58. M. Sajadi, T. Obernhuber, S. A. Kovalenko, M. Mosquera, B. Dick and N. P. Ernsting, *J. Phys. Chem. A*, 2009, **113**, 44-55.
59. M. Zhou, S. Long, X. Wan, Y. Li, Y. Niu, Q. Guo, Q.-M. Wang and A. Xia, *Phys. Chem. Chem. Phys.*, 2014, **16**, 18288-18293.
60. J. L. Pérez Lustres, S. A. Kovalenko, M. Mosquera, T. Senyushkina, W. Flasche and N. P. Ernsting, *Angew. Chem. Int. Ed.*, 2005, **44**, 5635-5639.
61. J. B. Asbury, Y. Wang and T. Lian, *Bull. Chem. Soc. Jpn.*, 2002, **75**, 973-983.
62. M. Sajadi, M. Weinberger, H.-A. Wagenknecht and N. P. Ernsting, *Phys. Chem. Chem. Phys.*, 2011, **13**, 17768-17774.

TOC Graphic

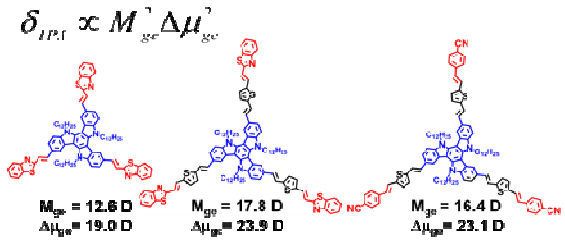

The intramolecular charge transfer properties of tribranched chromophores related to their TPA properties are explored by estimating the TPA essential factors.